Journal of
Nanoscience and Nanotechnology
Vol. 11, 6152–6156, 2011

RESEARCH ARTICLE

Broadband Antireflective Glasses with Subwavelength Structures Using Randomly Distributed Ag Nanoparticles

Gyeong Cheol Park[1], Young Min Song[1], Jong-Hoon Ha[1], and Yong Tak Lee[1, 2, 3, *]

[1] *Department of Information and Communications, Gwangju Institute of Science and Technology, Gwangju, 500-712, Republic of Korea*
[2] *Graduate Program of Photonics and Applied Physics, Gwangju Institute of Science and Technology, Gwangju, 500-712, Republic of Korea*
[3] *Department of Nanobio Materials and Electronics, Gwangju Institute of Science and Technology, Gwangju, 500-712, Republic of Korea*

We demonstrate broadband antireflective glasses with subwavelength structures (SWSs) using randomly distributed Ag nanoparticles. Ag nanoparticles formed by a thermal dewetting process were used as an etch mask for dry etching to fabricate antireflective SWSs on the glass surface. The size and shape of Ag nanoparticles are changed by the different thickness of the Ag thin film. The morphology of SWSs fabricated by using the Ag thin films is well consistent with that of the Ag nanoparticles. The single-side SWS integrated glass exhibits improved transmittance of ∼96% at 750 nm due to the graded refractive index profiles, while the transmittance is only ∼92.5% for the flat surface. To reduce Fresnel reflection at the other side of the glass substrate, the SWSs with optimized Ag film thickness and dry etching conditions are formed on both sides of the glass. The dual-side SWS integrated glass show an average transmittance of ∼97.5% in a wavelength range of 350–750 nm. Transmission band shrinkage effects of the SWS integrated glass are also observed with increased average size of the Ag nanoparticles.

Keywords: Metal Nanoparticles, Subwavelength Structures, Transparent Glass, Antireflection.

1. INTRODUCTION

Fresnel reflection occurring at the interface between two different materials is an undesirable effect, that degrades the optical performance in various optoelectronic devices including solar cells, light-emitting diodes, and photodetectors. It also causes deterioration of optical imaging systems including a reduction of transmitted light, and degradation of the legibility of the displays. Transparent glasses are one of the most important optical components for various optical imaging systems. Even though the refractive index of glasses is relatively lower than that of semiconductor materials, the index difference between the air and glass causes a reflectance of ∼8%, which degrades the performance of the optical system. To reduce the Fresnel reflection, antireflective (AR) coatings are commonly applied. However, this approach is hindered by numerous problems, such as thermal mismatch, adhesion, stability, and limitations of coating materials. In addition, many layers of thin films are required for broadband antireflective coatings. An alternative method has been found from the moth eye structure.[1–3] To obtain antireflective characteristics with a moth eye structure, the outermost surface of the devices in question should have periodic or aperiodic subwavelength structures (SWSs), which are surface relief structures smaller than the wavelength of the incident light.[4–14]

A number of methods to fabricate antireflective SWSs, including laser interference lithography, electron beam lithography, nanoimprint lithography, colloidal self assembly, and nanosphere lithography, have been reported.[4–14] However, these methods require sophisticated and costly fabrication procedures. Recently, randomly distributed metal nanoparticles have been developed for use as an nanoscale etch mask.[15–17] This method is simple and cost-effective compared to conventional lithography processes. Moreover, the average size and shape of nanoparticles can be varied by changing the film thickness and

*Author to whom correspondence should be addressed.

 1533-4880/2011/11/6152/005 doi:10.1166/jnn.2011.4350

annealing temperature. In this paper, we have fabricated SWSs on glass substrates using randomly distributed Ag nanoparticles to reduce the surface reflection of the glasses in a broad wavelength range. Antireflective SWSs were fabricated by an overall dry etch process using Ag nanoparticles. The transmittance characteristics of fabricated single- and dual-side SWS integrated glasses with different process conditions were also shown along with theoretical explanations.

2. EXPERIMENTAL DETAILS

The fabrication procedure for antireflective SWSs on a glass surface is schematically shown in Figure 1. The glass used in this experiment was 500-μm-thick borosilicate glass (Schott borofloate 33) with a 2 cm × 2 cm squared shape. Prior to the deposition of Ag thin films on the glass surface, the samples were cleaned with acetone, methanol, and deionized water with the use of ultrasonic agitation Ag thin films with thicknesses of 10 nm, 15 nm, and 20 nm were deposited on the samples, respectively, by using an ebeam evaporator. In order to form Ag nanoparticles using the dewetting process, a rapid thermal annealing process was subsequently carried out at 500 °C for 1 min under a nitrogen atmosphere. To fabricate SWSs with a tapered profile, an overall dry etch process was conducted by using inductively coupled plasma (ICP) under a SF_6/O_2 (40 sccm/10 sccm) gas mixture at ICP power of 200 W and RF power of 100 W for 2 min, 3 min, and 4 min, respectively. During the dry etch process, Ag nanoparticles were used as a nanoscale etch mask. Lastly, to remove the residual Ag nanoparticles, the samples were dipped into a nitric acid (HNO_3) for 2 min.

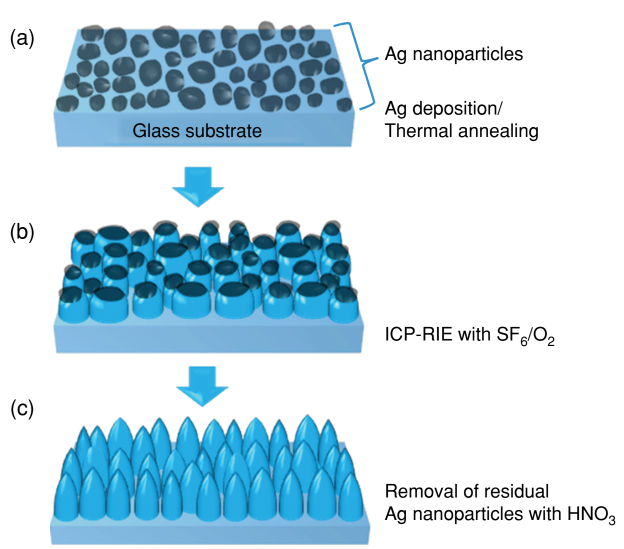

Fig. 1. Schematic illustration of the fabrication procedure for antireflective SWSs on the glass surface using randomly distributed Ag nanoparticles.

To verify the effects of the antirefletive SWSs, we fabricated SWSs on single- and dual-side glasses, respectively. The morphology of Ag nanoparticles with different film thicknesses and the fabricated SWSs on glass substrates were observed using a field-emission scanning electron micoscope (FE-SEM, S-4700, Hitachi) with an accelerating voltage of 15 kV. The transmittance measurement of bare glass specimens and SWS integrated glasses was carried out using a UV-VIS-NIR spectrophotometer (Cary 5000, Varian, USA) equipted with an integrating sphere in a wavelength range of 350–750 nm at an interval of 1 nm Deuterium arc and tungsten halogen were used as an UV and visible light source, respectively. As a photodetector, high performance R928 photomultiplier tube were used. The absolute values are obtained from the ratio of the sample spectrum and reference spectrum. The reported transmittance are the average values of several data obtained from various spots of identical sample.

3. RESULTS AND DISCUSSION

The average diameter and area fraction of Ag nanoparticles can be changed by the thickness of the Ag thin film and the annealing temperature of the dewetting process.[18, 19] Figure 2 shows SEM images of the Ag thin films on glass substrates annealed at 500 °C for 1 min under a nitrogen atmosphere, for film thicknesses of (a) 10 nm, (c) 15 nm, and (e) 20 nm, respectively. As shown in Figure 2(a), the shape of the Ag nanoparticles is nearly circular. However, with increasing film thickness, the morphology gradually becomes shapeless. In the case of the Ag thin film with a thickness of 20 nm, the surface energy of the thin film was not sufficient to allow the nanoparticles to agglomerate into circular shaped nanoparticles.[19] To analyze the morphology of randomly distributed Ag nanoparticles, we calculated the average diameter and area fraction of Ag nanoparticles in SEM images using a commercial image processor (ImageJ 1.43u, NIH).[18, 20] To obtain accurate information, SEM images with 256-level gray scales were converted to binary images by adjusting a threshold level. The average diameter d were simply calculated by $A = \pi(d/2)^2$, where A is an area of each nanoparticle. The area fraction was deduced by the ration of black and white area in the binary image. Figures 2(b, d, f) shows the diameter distribution of Ag nanoparticles with different deposited film thickness. The measured average diameters of Ag nanoparticles with film thicknesses of 10, 15 and 20 nm were 88 ± 74, 108 ± 83, and 181 ± 151 nm, respectively. Because the transmission spectra can be affected by the average diameter of the SWSs, the film thickness should be carefully chosen. For a glass substrate, a grating period of below 200 nm is needed to remove higher order diffraction,[21] and Ag film thickness of <15 nm is adequate for broadband antireflective SWSs. The average area fractions of Ag nanoparticles with film thicknesses of

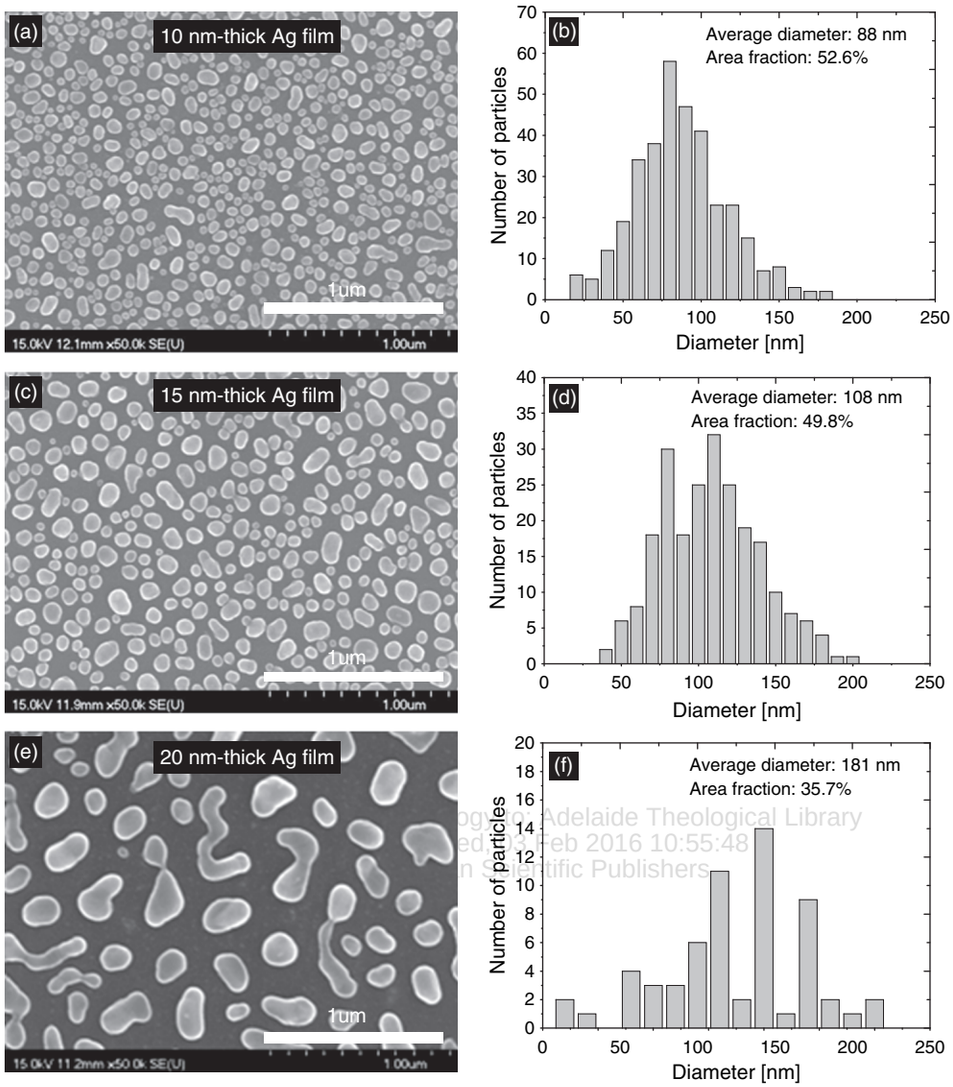

Fig. 2. Surface morphologies and diameter distributions of Ag nanoparticles on glass substrates (a, c, e) SEM images of Ag films with thicknesses of (a) 10 nm, (c) 15 nm, and (e) 20 nm after thermal annealing at 500 °C for 1 min and (b, d, f) corresponding diameter distribution of Ag nanoparticles.

10 and 15 nm have similar values of ∼50%; however, as the film thickness increases from 15 nm to 20 nm, the average fractions rapidly changed from 49.8% to 35.7%. Since low packing density degrades the antireflection property due to an abrupt refractive index change, film thickness of >20 nm is not sufficient for antireflection.

Figure 3 shows SEM images of the fabricated SWSs on the glass substrates with different etch times and different thicknesses of Ag thin films. As expected, the average distance between the nearest SWSs using 15 nm thick Ag film is much smaller than that of SWSs using 20 nm thick Ag film, showing a similar tendency to that depicted in Figure 2. As the etching time is increased from 2 min to 4 min, the heights of SWSs using 15 nm-thick Ag films vary from 280 to 360 nm. On the other hand, increased heights (280–550 nm) are observed in the SWSs using 20 nm-thick Ag films. This can be attributed to the effects of the packing density on the etch rate. As depicted in Figure 3, the shape of the SWSs is also slightly changed as the etch time changes.

In order to evaluate the optical characteristics of the SWS integrated glasses with different processing conditions, the transmittance of bare and SWS integrated glasses was measured using a UV-VIS-NIR spectrophotometer in a wavelength range of 350–750 nm at normal incidence. Figure 4 shows the measured transmittance of the bare glass and single-side SWS integrated glasses fabricated using Ag nanoparticles with thicknesses of (a) 15 nm and (b) 20 nm. The glasses with single-side SWS yield transmittance of 95–96% at 750 nm due to the graded refractive index profiles, while the transmittance is only ∼92.5% for the flat surface. The difference in the transmittance

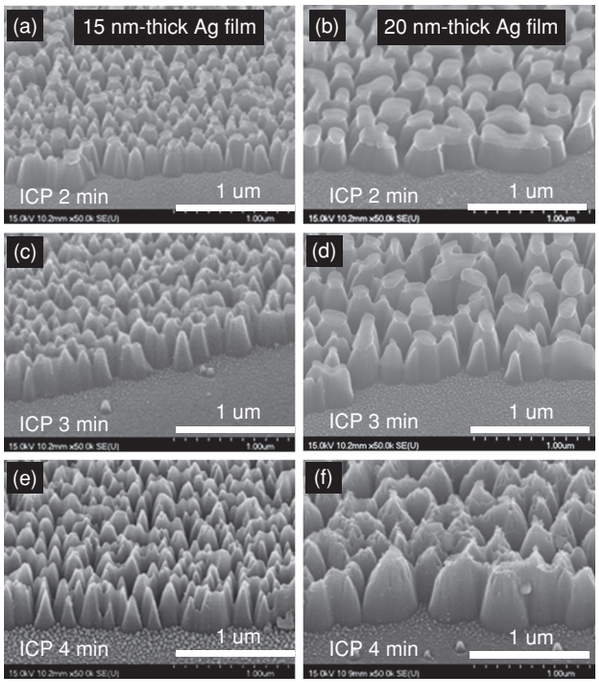

Fig. 3. SEM images of the fabricated SWSs with overall dry etch process for (a, b) 2 min, (c, d) 3 min, and (e, f) 4 min using 15 nm-thick (a, c, e) and 20 nm-thick (b, d, f) Ag films.

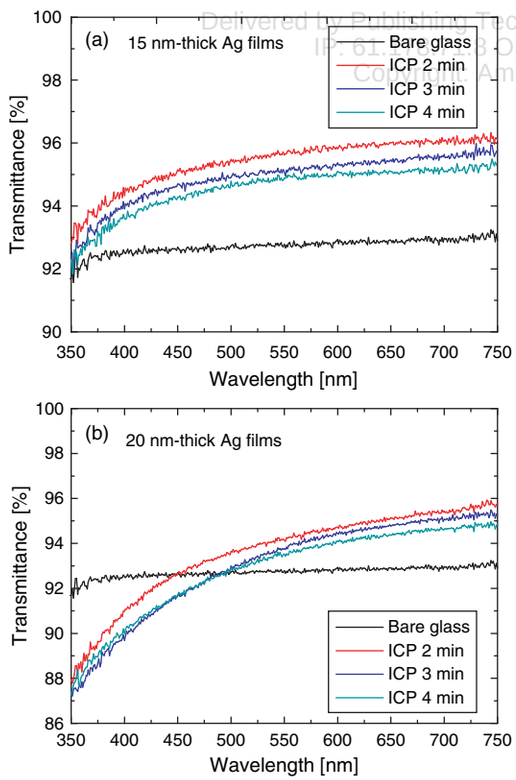

Fig. 4. Measured transmittance of single-side SWS integrated glasses fabricated by Ag nanoparticles with thicknesses of (a) 15 nm and (b) 20 nm under different dry etch times. The measured transmittance for a bare glass sample is also shown as a reference.

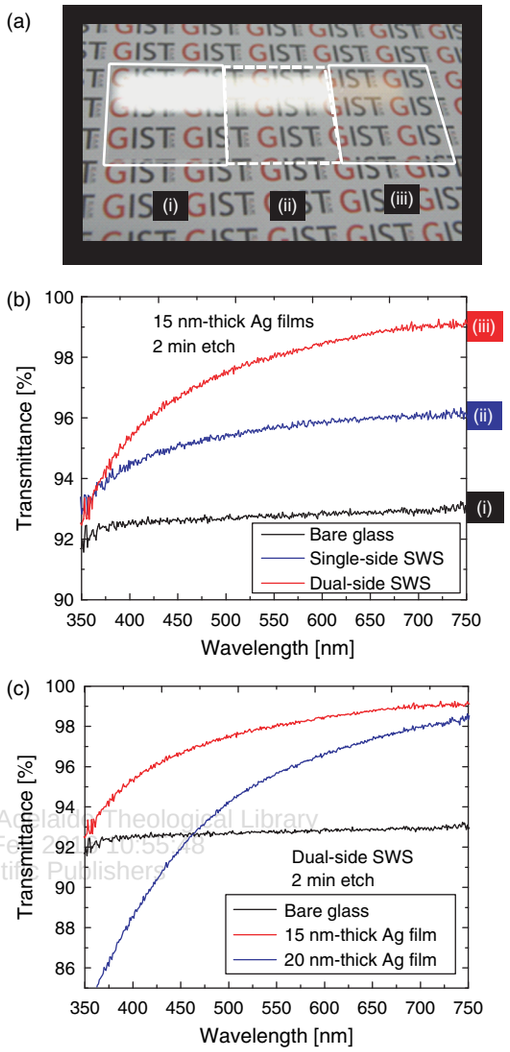

Fig. 5. (a) Photograph of (i) bare glass and (ii) single- and (iii) dual-side SWS integrated glass. (b) Measured transmittance of single- and dual-side SWS integrated glasses fabricated by Ag nanoparticles with a thickness of 15 nm. The measured transmittance for a bare glass sample is also shown as a reference. (c) Measured transmittance of dual-side SWS integrated glasses fabricated by Ag nanoparticles with thicknesses of 15 nm and 20 nm for 2 min dry etch process.

between the SWSs with different etch times is less than 1% throughout the visible range. As the etch time is increased, the heights of the SWSs are increased, which is favorable for broadband antireflection. However, the packing fraction is also decreased during the dry etch process, which degrades the antireflection property due to an increased index difference between the glass and SWSs. Furthermore, the results are consistent with finding that SWSs with a truncated cone shape show better antireflection performance compared to that of SWSs with a cone shape at certain height ranges.[21] For the SWSs using 15 nm-thick Ag films, the transmittances are slightly decreased at shorter wavelength ranges but still sustained higher values

RESEARCH ARTICLE

than that of a flat surface. For the SWSs using 20 nm-thick Ag films, however, a rapid drop of the transmittance is observed at short wavelength ranges and the transmittance was even lower than that of bare glass. These transmission band shrinkage effects are affected by the large distance between Ag nanoparticles, which provides higher order diffractions.[21]

For greater increment of the transmittance, SWSs produced under optimized conditions were fabricated on both sides of the glass substrate. Figure 5(a) shows photographs of (i) bare glass and (ii) single- and (iii) dual-side SWS integrated glass exposed to a fluorescent lamp. As shown in Figure 5(a), the bare glass shows poor readability due to strong reflection at both surfaces. The single-side SWS integrated glass exhibits poor legibility due to Fresnel reflection at the other side. The dual-side SWS integrated glass, however, demonstrates high-quality transparency and little reflection loss. Figure 5(b) shows the transmittance of the single-side and dual-side SWS integrated glasses fabricated using Ag nanoparticles with 15 nm thickness. In the dual-side SWS integrated glass, the increment of transmittance was increased nearly twofold compared to that of the single-side SWS integrated glass and average transmittance of 97.5% was achieved. For comparison, we also fabricated dual-side SWS integrated glass specimens using 20 nm-thick Ag films. As depicted in Figure 5(c), there still exists a rapid drop of transmittance at short wavelength ranges for the SWSs using 20 nm-thick Ag films. Also, the drop point is similar with the case of single-side SWS integrated glasses. Therefore, SWSs with average period below 200 nm are required for broadband antireflective glasses.

4. CONCLUSIONS

To reduce the Fresnel reflection at the interfaces of the air and glass, we fabricated SWS integrated glasses by an overall dry etch process using Ag nanoparticles, which are formed by thermal dewetting. By applying the SWSs on both sides of the glass with optimized Ag film thickness and dry etching conditions, average transmittance of ∼97.5% was achieved in the entire visible wavelength region. From these results, we believe that highly transparent glasses fabricated by this simple and cost-effective method have strong potential for displays, projection optics, and other optical imaging systems.

Acknowledgments: This work was partially supported by the Systems biology infrastructure establishment grant provided by GIST, by the World Class University (WCU) program at GIST through a grant provided by MEST of Korea (R31-20008-000-10026-0).

References and Notes

1. Y. M. Song, S. J. Jang, J. S. Yu, and Y. T. Lee, *Small* 6, 984 (**2010**).
2. B. J. Bae, S.-H. Hong, E.-J. Hong, H. Lee, and G.-Y. Jung, *Jpn. J. Appl. Phys.* 48, 010207 (**2009**).
3. A. Kaless, U. Schulz, P. Munzert, and N. Kaiser, *Surf. Coat. Technol.* 200, 58 (**2005**).
4. Y. Kanamori, H. Kikuta, and K. Hane, *Jpn. J. Appl. Phys.* 39, 735 (**2000**).
5. Y. H. Kang, S. S. Oh, Y.-S. Kim, and C.-G. Choi, *Microelectron. Eng.* 87, 125 (**2010**).
6. Z. Yu, H. Gao, W. Wu, H. Ge, and S. Y. Chou, *J. Vac. Sci. Technol. B* 21, 2874 (**2003**).
7. C.-H. Sun, P. Jiang, and B. Jiang, *Appl. Phys. Lett.* 92, 061112 (**2008**).
8. W.-L. Min, B. Jiang, and P. Jiang, *Adv. Mater.* 20, 1 (**2008**).
9. Y. Li, J. Zhang, S. Zhu, H. Dong, Z. Wang, Z. Sun, J. Guo, and B. Yang, *J. Mater. Chem.* 19, 1806 (**2009**).
10. Gombert, W. Glaubitt, K. Rose, J. Dreibholz, B. Bläsi, A. Heinzel, D. Sporn, W. Döll, and V. Wittwer, *Thin Solid Films* 35, 73 (**1999**).
11. Y.-F. Huang, S. Chattopadhyay, Y.-J. Jen, C.-Y. Peng, T.-A. Liu, Y.-K. Hsu, C.-L. Pan, H.-C. Lo, C.-H. Hsu, Y.-H. Chang, C.-S Lee, K.-H Chen, and L.-C. Chen, *Nat. Nanotechnol.* 2, 770 (**2007**).
12. M. Ibn-Elhaj and M. Schadt, *Nature* 410, 796 (**2001**).
13. H. Y. Koo, D. K. Yi, S. J. Yoo, and D.-Y. Kim, *Adv. Mater.* 16, 274 (**2004**).
14. Z. Wu, J. Walish, A. Nolte, L. Zhai, R. E. Cohen, and M. F. Rubner, *Adv. Mater.* 18, 2699 (**2006**).
15. K. H. Baek, J. H. Kim, K. B. Lee, H. S. Ahnn, and C. S. Yoon, *J. Nanosci. Nanotechnol.* 10, 3118 (**2010**).
16. B. Park, K. Cho, J. Yun, Y.-S. Koo, J.-H. Lee, and S. Kim, *J. Nanosci. Nanotechnol.* 9, 1904 (**2009**).
17. Y. M. Song, E. S. Choi, J. S. Yu, and Y. T. Lee, *Opt. Express* 17, 20991 (**2009**).
18. Y. Kojima and T. Kato, *Nanotechnology* 19, 255605 (**2008**).
19. J.-M. Lee and B.-I. Kim, *Mater. Sci. Eng. A* 449–451, 769 (**2007**).
20. E. S. Kooji, E. A. M. Brouwer, H. Wormeester, and B. Poelsema, *Langmuir* 18, 7677 (**2002**).
21. Y. M. Song, H. J. Choi, J. S. Yu, and Y. T. Lee, *Opt. Express* 18, 13063 (**2010**).

Received: 8 July 2010. Accepted: 16 January 2011.